Effects of the Nature of the Metal Ion, Protein and Substrate on the Catalytic Center in Matrix Metalloproteinase-1: Insights from Multilevel MD, QM/MM and QM Studies

Ann Varghese,[a] Shobhit S. Chaturvedi,[a] Bella DiCastri,[a] Emerald Mehler,[b] Gregg B. Fields,[c] and Tatyana G. Karabencheva-Christova[a*]

[a]Department of Chemistry, Michigan Technological University, Houghton, Michigan 49931

[b]Department of Chemical Engineering, Michigan Technological University, Houghton, Michigan 33458

[b]Department of Chemistry and Biochemistry and I-HEALTH, Florida Atlantic University, Jupiter, Florida 33458

Table of Contents

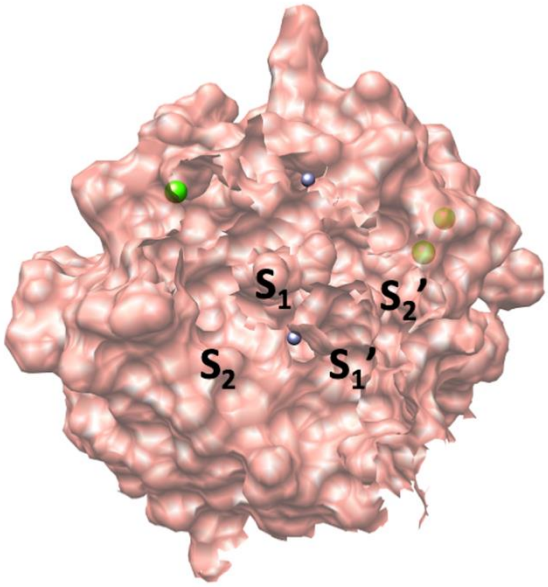

Figure S1. Subsite locations in the CAT domain of MMP-1.

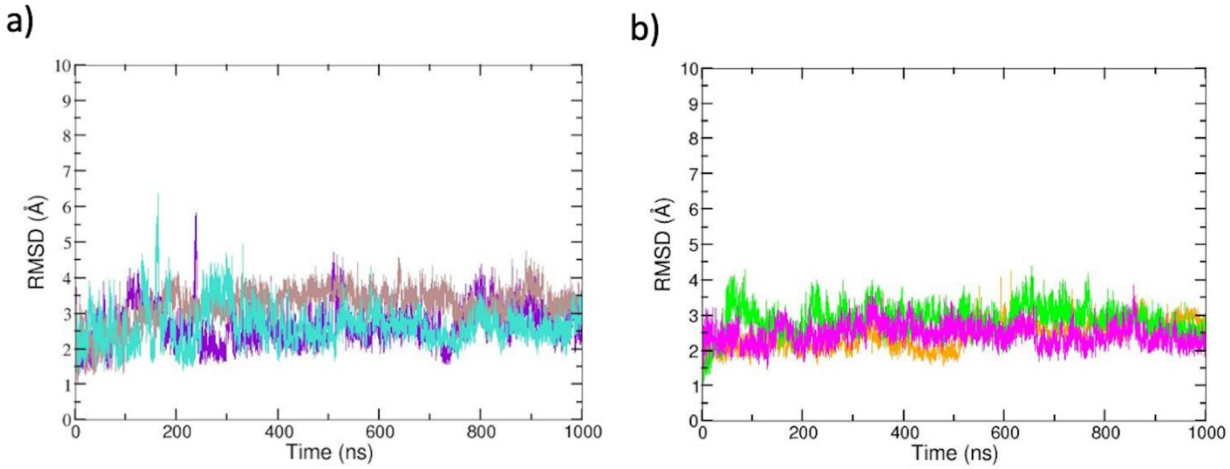

Figure S2. Multiple trajectories of a) MMP-1•no THP and b) MMP-1•Co_1•THP. The single trajectory used for further calculations is depicted in violet for MMP-1•no THP and yellow for MMP-1•Co_1•THP.

Table S1: Cosine content of the first three PC's of the trajectories of MMP-1•no THP and MMP-1 Co_1•THP. Cosine content value less than 0.5 is indicative of good sampling.

PC's	MMP-1•no THP	MMP-1 Co_1•THP
PC1	0.08	0.57
PC2	0.00	0.03
PC3	0.03	0.13

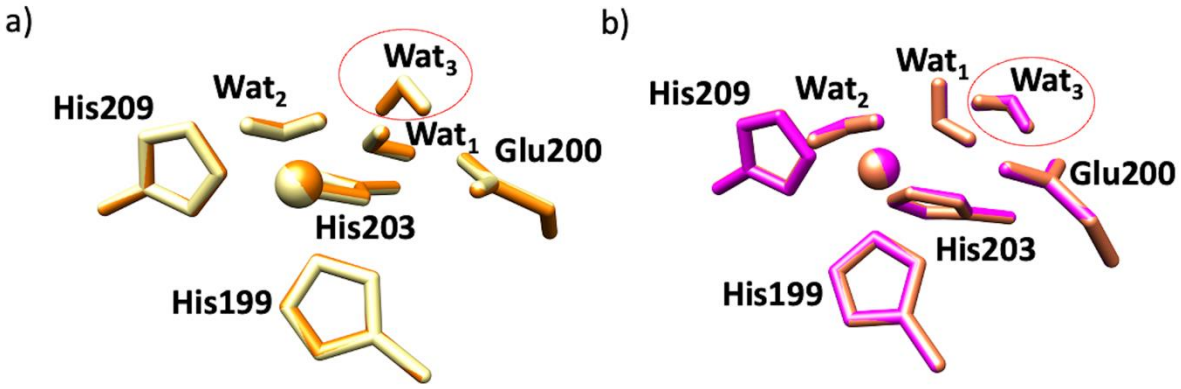

Figure S3: Superimposed catalytic Zn(II)/Co(II) site of a) MMP-1•no THP with Wat_3 in the QM site (khaki) and MM region (orange) b) MMP-1 Co_1•no THP with Wat_3 in the QM site (coral) and MM region (magneta).

Conformational Analysis of MMP-1•THP

We calculated the distances between various important sites in the domains of MMP-1. Comparing the distances as in Table S2, it was identified that the distances between the center of mass of the catalytic site and the scissile bond in the MD trajectory and the QM/MM optimized structure are in good accord with the X-ray crystallographic structure of the enzyme. However, a more

significant deviation in the distance between the catalytic and the structural site ranging from 13.93 – 14.39 Å was noticed. In addition, we calculated the distance between the center of mass of CAT and HPX domains. The crystallographic structure of the enzyme provided a distance of 38.71 Å between the domains, which showed a minor increase to 38.94 Å during the MD simulation. QM/MM calculations provided the distance between the domains in good agreement with the crystallographic structure.

Table S2. Distances between the center of mass of catalytic site and scissile bond, the center of mass of catalytic and structural site, and the center of mass of the CAT and HPX domains compared among the X-ray crystallographic structure, MD trajectory, and QM/MM model of MMP-1•THP.

	Distance (Å)		
	Crystal structure	MD	QM/MM
Center of mass of catalytic site and scissile bond	8.44	8.52	8.50
Center of mass of catalytic and structural site	13.93	14.39	14.06
Center of mass of CAT and HPX domains	38.71	38.94	38.78

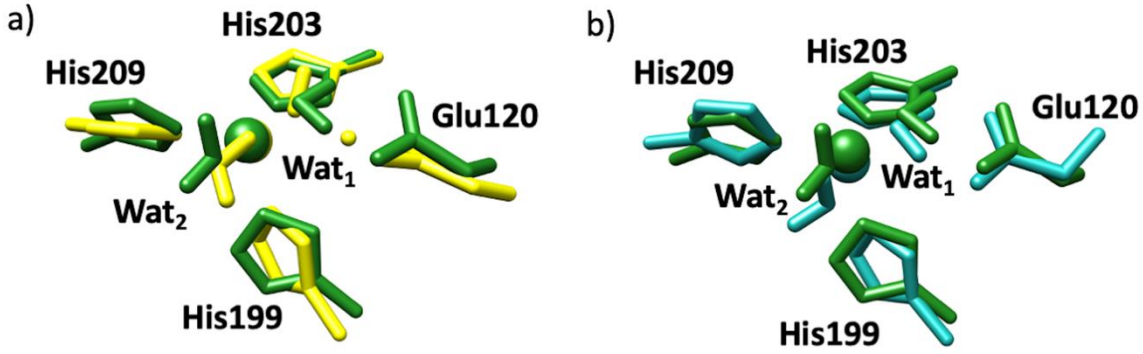

Figure S4. Superimposed catalytic Zn(II) site of MMP-1•THP in the QM/MM optimized structure (green) and the a) QM-only (yellow) and b) QM-continuum model (ocean blue).

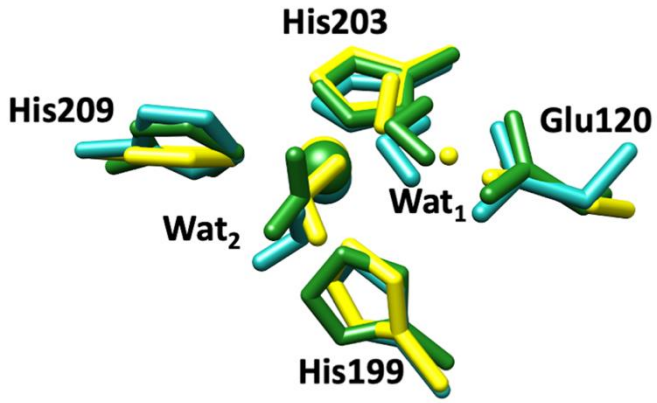

Figure S5. Superimposed catalytic Zn(II) site of MMP-1•THP in the QM/MM optimized geometry (green) with the QM-only (yellow) and QM-continuum model (ocean blue).

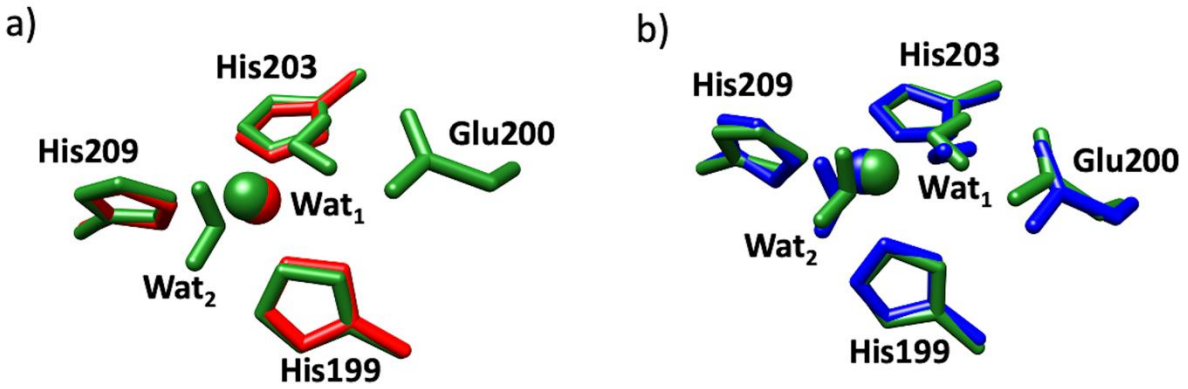

Figure S6. Catalytic site of MMP-1•THP. a) Superimposed catalytic site in the QM/MM optimized structure (green) and X-ray crystallographic structure (red). b) Superimposed catalytic site in the QM/MM optimized structure (green) and MD snapshot (blue).

Mulliken Charge Distribution in MMP-1•THP

The Mulliken charge distribution in the catalytic site of MMP-1was analyzed to learn more about the nature of Zn(II) coordination. Table S3 represents the Mulliken charges for the Zn(II) and the coordinated histidines in the catalytic site. Both QM/MM and QM-continuum models display Zn(II) as a center of positive charge. The electrostatic embedding scheme for QM/MM shows a slightly higher electropositivity of 0.84. The electronegativity of nitrogen atoms of histidine residues coordinated to the catalytic Zn(II) calculated by the population analysis is almost identical for both models.

Table S3**.** Mulliken charges of catalytic Zn(II) coordinated residues in the QM/MM and QM-continuum approach for MMP-1•THP.

Atoms	Charge	
	QM/MM	QM/continuum
Zn(II)	0.84	0.81
His199-NE2	-0.29	-0.27
His203 - NE2	-0.28	-0.27
His209-NE2	-0.29	-0.28

Table S4. Distances between catalytic Zn(II) and the coordinated histidine residues in multiple snapshots (snapshot 1 chosen for further calculations) of the QM/MM optimized geometry of MMP-1•THP.

Atoms		Bond length (Å)				
		Snapshot 1	Snapshot 2	Snapshot 3	Snapshot 4	Snapshot 5
Zn(II)	His199-NE2	2.06	2.06	2.08	2.05	2.07
Zn(II)	His203-NE2	2.19	2.18	2.14	2.14	2.18
Zn(II)	His209-NE2	2.05	2.04	2.07	2.03	2.08

Table S5. Angles between the catalytic Zn(II) ion and the coordinated histidine residues in multiple snapshots (snapshot 1 chosen for further calculations) of the QM/MM optimized geometry of MMP-1•THP.

Atoms			Angle (°)				
			Snapshot 1	Snapshot 2	Snapshot 3	Snapshot 4	Snapshot 5
His199-NE2	Zn(II)	His203-NE2	103.33	98.46	102.97	101.29	98.85
His203-NE2	Zn(II)	His209-NE2	93.73	94.86	95.53	95.47	94.10
His199-NE2	Zn(II)	His209-NE2	108.67	111.08	106.08	111.52	107.10

Investigating the effects of the substrate in MMP-1

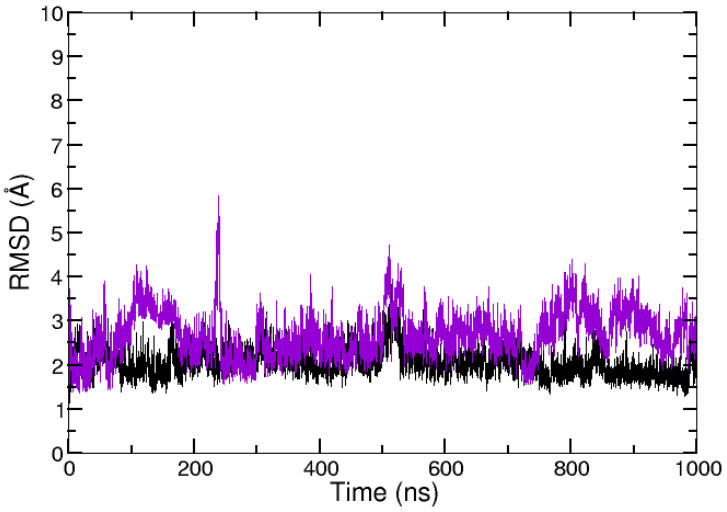

Figure S7. RMSD of MMP-1•THP (black) and MMP-1•no THP (violet).

Principal Component Analysis and Dynamic Cross-Correlation Analysis of MMP-1•no THP

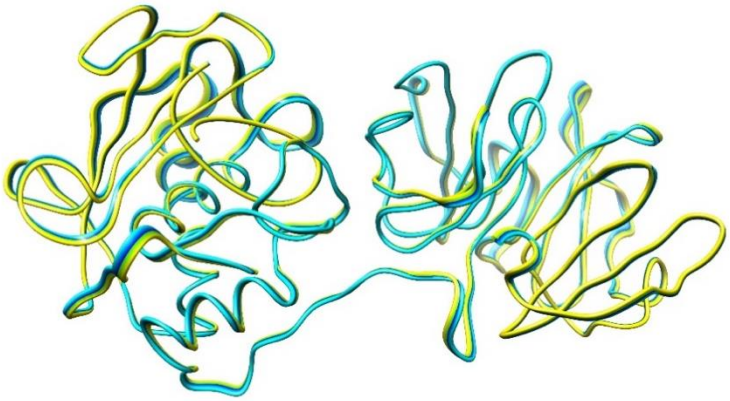

Figure S8. Principal component analysis of MMP-1•no THP. Yellow to blue represents the direction of motion.

Table S6. Distances between Zn(II) and coordinating residues in the catalytic site in the QM/MM analysis of MMP-1•THP and MMP-1•no THP.

Atoms		Bond length (Å)	
		MMP-1•THP	MMP-1•no THP
Zn(II)	His199-NE2	2.06	2.07
Zn(II)	His203-NE2	2.19	2.18
Zn(II)	His209-NE2	2.05	2.08

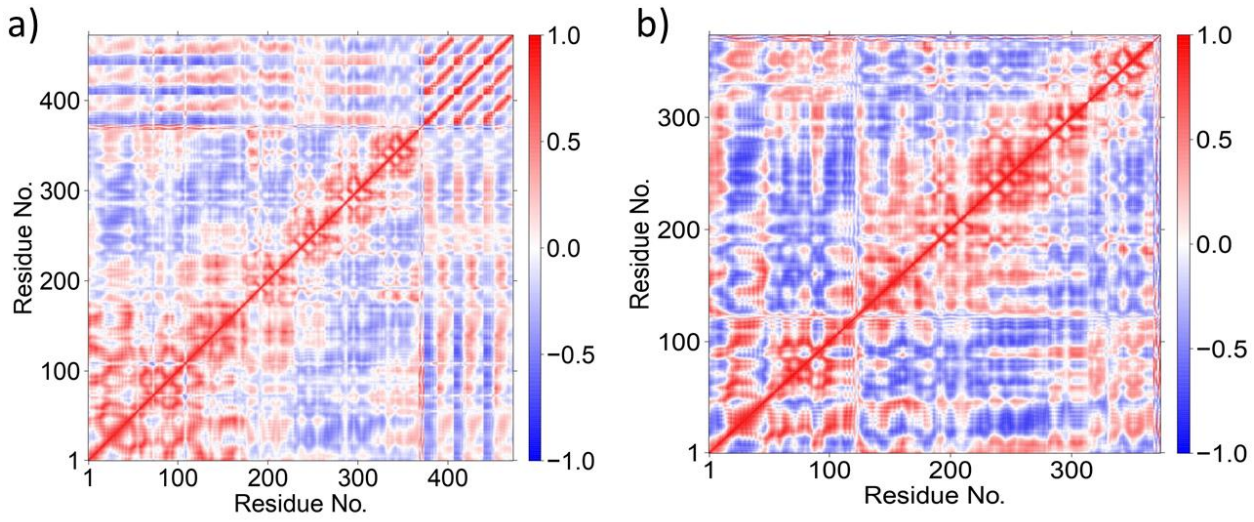

Figure S9. Dynamic cross-correlation analysis of a) MMP-1•THP, and b) MMP-1•no THP. Red color represents positive correlation and blue represents anti-correlation.

Table S7. Angles between the catalytic Zn(II) ion and the coordinated histidines in the QM/MM approach for MMP-1•THP and MMP-1•no THP.

Atoms			Angle (degrees) (QM/MM)	
			MMP-1•THP	MMP-1•no THP
His199-NE2	Zn(II)	His203-NE2	103.33	101.93
His203-NE2	Zn(II)	His209-NE2	93.73	92.32
His199-NE2	Zn(II)	His209-NE2	108.67	113.70

Table S8. Hydrogen bonding interaction in the QM/MM optimized geometry of the catalytic and structural site of MMP-1•THP and MMP-1•no THP.

Atoms			Bond length (Å)	
Donor	Donor H	Acceptor	MMP-1•THP	MMP-1•no THP
CATALYTIC SITE				
His199-ND1	His199-HD1	Leu216-O	2.82	2.75
His199-ND1	His199-H	Arg195-O	Not present	2.91
His203-N	His203-H	Glu200-O	2.74	2.75
His209-N	His209-H	Ser208-OG	2.85	Not present
STRUCTURAL SITE				
His177-N	His177-H	His164-O	2.81	2.82
His164-N	His164-H	His177-O	2.92	3.05
Ser153-N	Ser153-H	Asp151-O	2.78	Not present
Ser153-N	Ser153-H	Asp151-OD1	Not present	2.88

Conformational Analysis of MMP-1 Co_1•THP

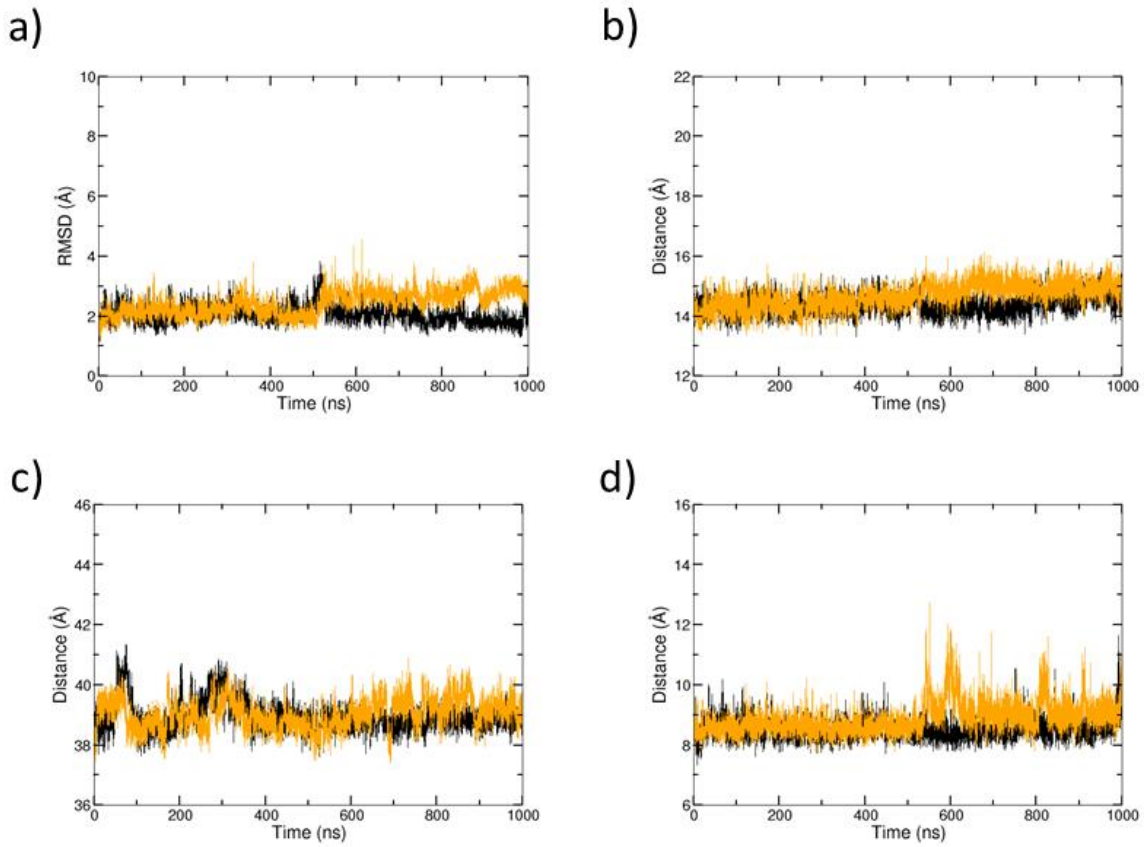

Figure S10. Comparison of a) RMSD, b) distance between the center of mass of catalytic Zn(II)/Co(II) and structural Zn(II) bonded residues, c) distance between the center of mass of the CAT and HPX domains, and d) distance between the center of mass of catalytic site and the scissile bond between MMP-1•THP (black) and MMP-1 Co_1•THP (orange).

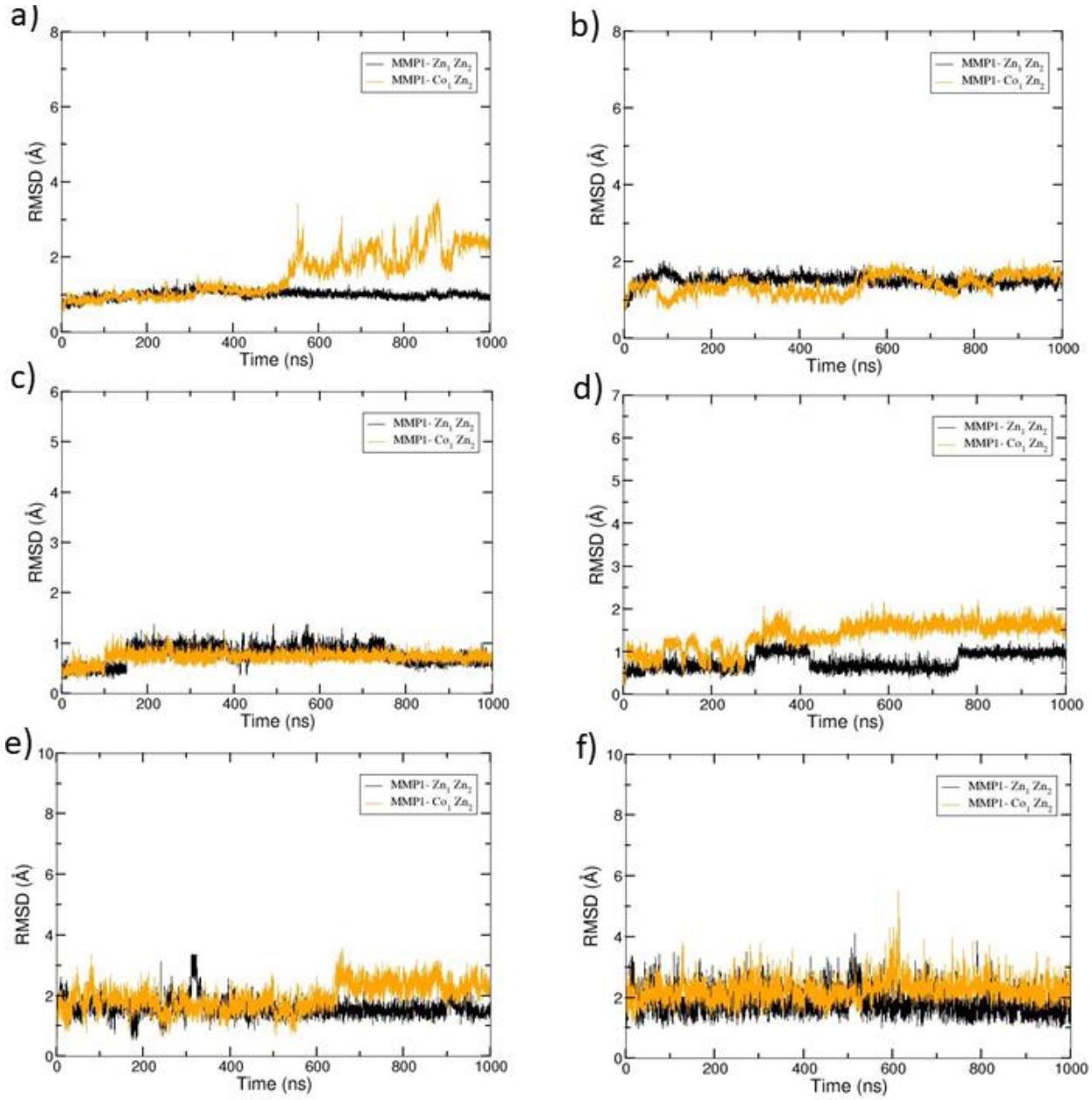

Figure S11. Superimposed RMSDs of MMP-1•THP (black) and MMP-1 Co_1•THP (orange). RMSD of a) CAT domain, b) HPX domain, c) S-loop, d) V-B loop, e) linker, and f) THP.

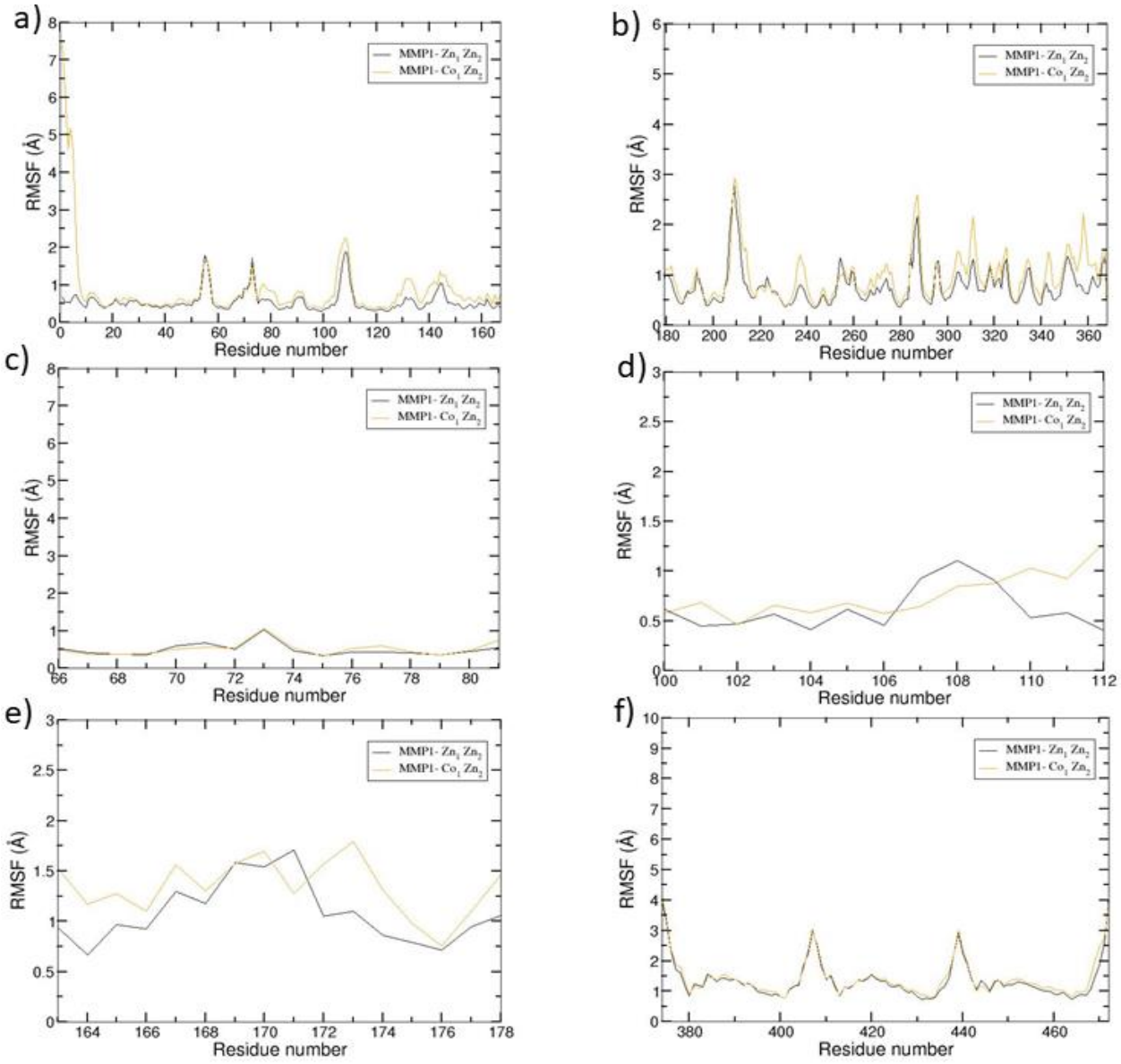

Figure S12. Superimposed RMSFs of MMP-1•THP (black) and MMP-1 Co_1•THP (orange). RMSF of the a) CAT domain [residue numbering corresponds to the X-ray crystallographic structure (PDB ID: 4AUO) numbering 81-242 and incorporating the Zn(II), Co(II), and Ca(II) ions], b) HPX domain [residue numbering corresponds to the X-ray crystallographic structure numbering 259-447 and incorporating the Ca(II) ion], c) S-loop [residue numbering corresponds to 146-161], d) V-B loop [residue numbering corresponds to the X-ray crystallographic structure numbering 180-192], e) linker [residue numbering corresponds to crystal structure numbering 243-258], and f) THP [residue numbering corresponds to X-ray crystallographic structure numbering 963-995].

Dynamic Cross-correlation Analysis and Principal Component Analysis of MMP-1 Co_1•THP

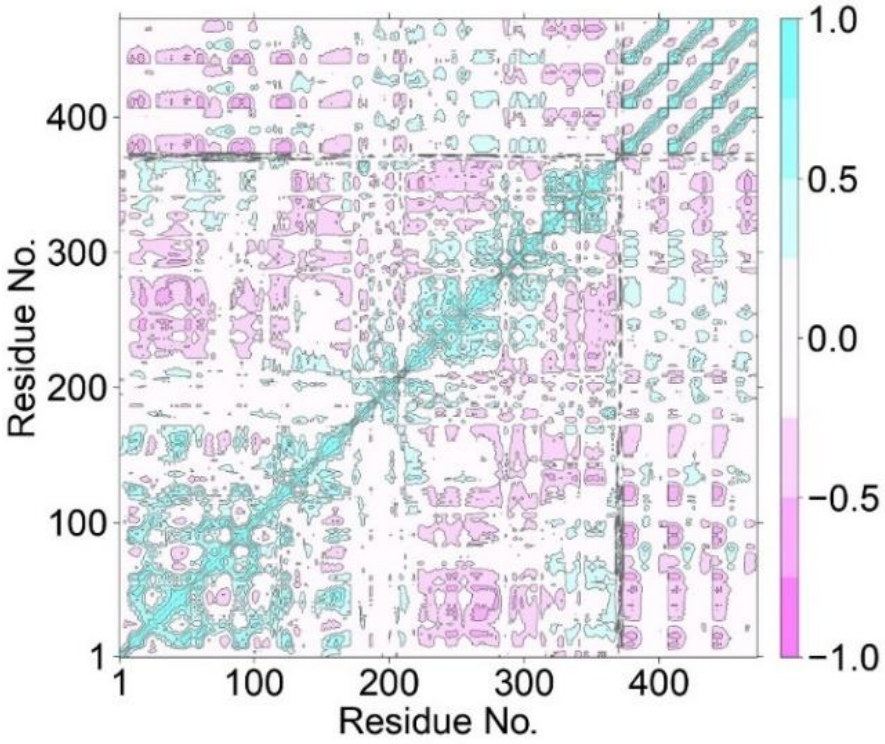

Figure S13. Dynamic Cross-Correlation Analysis of MMP-1 Co_1•THP.

The DCCA of MMP-1 Co_1•THP showed a positive correlation between the S_{10}' exosite and the S_1' specificity loop. However, the correlations were exhibited by a lesser span of exosite residues (282-283 and 292-300) compared to MMP-1•THP.[1] The Zn(II) ion in the catalytic site might have the specific role of maintaining these positive correlations. HPX blade 2 residues (except 302 and 304) showed no correlation to the S_1' specificity loop. The blade residues retained their anti-correlating property with the V-B loop. However, only a minor segment of the S-loop was involved in anti-correlation with the blade residues (331-333 and 338-341). The positive correlation of the structural Zn(II) and catalytic site metal ion with the S loop residues were not affected by Co(II) substitution. The structural Zn(II) had positive correlations with a lower fraction of V-B loop

residues upon Co(II) substitution (179-184 and 193). The same trends were seen with catalytic site metal ion and the V-B loop residues for Zn(II) and Co(II) (179 and 191-193). In contrast, the anti-correlation of Arg189 with the structural Zn(II) was lost upon Co(II) substitution. While some correlations in MMP-1•THP disappeared in the Co(II) engineered enzyme, correlated motions involving a larger number of residues were observed in some parts.[1] For example, most of the V-B loop residues were involved in a positive correlation with the S-loop. The conserved Gly252 of the linker lost the positive correlation with the catalytic Co(II) bound residues and the S_1' specificity loop. A loss of anti-correlation was observed between the scissile peptide bond residues Gly775 and Leu776 and the structural Zn(II). The loss of correlated motions on the replacement of Zn(II) by Co(II) may affect the structural characteristics of the enzyme but not the catalytic efficiency, as Co(II)-substituted metalloproteinases are capable of catalytic activity. A new correlation seen in the Co(II) system in contrast to MMP-1•THP was the anti-correlation between the V-B loop (residues 181-188) and *N*-terminal loop residues (88-91).[1] The THP leading (L) strand residues (767-774) developed a positive correlation with residues 324-330 of blade 2 upon substitution with Co(II). These results point towards the allosteric control of the catalytic Zn(II). THP-THP interactions observed were similar to MMP-1•THP.

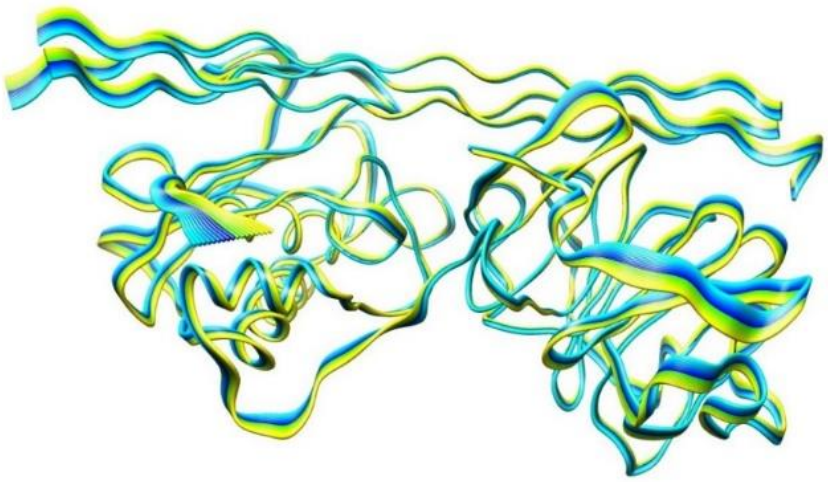

Figure S14. Principal Component Analysis of MMP-1 Co_1•THP. PCA of the Co(II)-substituted MMP-1•THP complex indicated that the HPX domain exhibited more flexible movements compared to CAT domain. The N-terminal loop showed vigorous movements. The linker region near CAT domain moved in the same direction as CAT domain while the linker region near the HPX domain moved similar to the domain. Flexible movements were observed in the linker.

Investigating the effects of the substrate in cobalt substituted MMP-1

Table S9. Spin densities of the ligands in the QM/MM catalytic site of MMP-1 Co_1•THP

Ligands	Spin Density
Co(II)	2.82
His191	0.03
Glu200	0.00
His203	0.03
His209	0.03

Table S10. Distances between Co(II) and the coordinating residues in MMP-1 Co_1•THP and MMP-1 Co_1•no THP in the QM/MM optimized structure.

Atoms		Distance (Å)	
		MMP-1 Co_1•THP	MMP-1 Co_1•no THP
Co(II)	His199-NE2	2.07	2.09
Co(II)	His203-NE2	2.11	2.11
Co(II)	His209-NE2	2.09	2.04

Table S11. Angles between Co(II) and the coordinating residues in MMP-1 Co_1•THP and MMP-1 Co_1•no THP in the QM/MM optimized structure.

Atoms			Angle (degrees)	
			MMP-1 Co_1•THP	MMP-1 Co_1•no THP
His199-NE2	Co(II)	His203-NE2	105.39	100.24
His203-NE2	Co(II)	His209-NE2	96.70	101.57
His199-NE2	Co(II)	His209-NE2	107.71	105.07

Bond lengths and bond angles of the catalytic Co(II) and the coordinated histidines of the MMP-1 Co_1•THP and MMP-1 Co_1•no THP in the QM/MM approach were calculated (Tables S10 and S11). The THP did not likely influence the active site bonds. The MD and QM/MM optimized structure bond lengths remained approximately constant. The angles involved with the catalytic site showed a different trend. The binding of the THP resulted in larger angles between His199 – Co(II) – His203 (105.39°) and His199 – Co(II) – His209 (107.71°). In contrast, the angle between His203 – Co(II) – His209 decreased from 101.57° in MMP-1 Co_1•no THP to 96.70° in MMP-1 Co_1•THP.

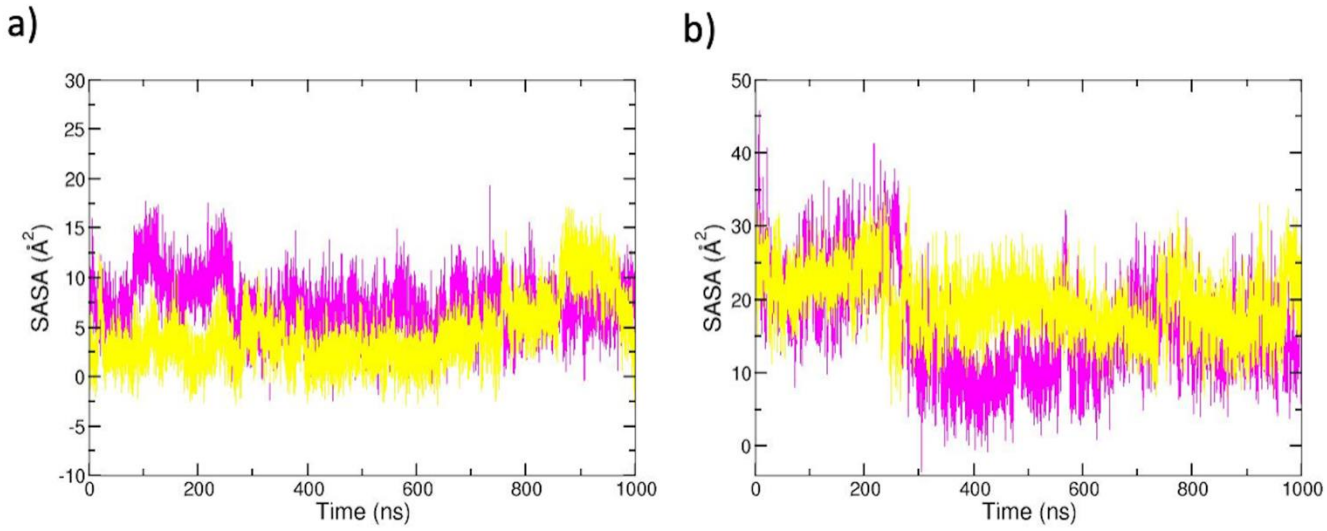

Figure S15: SASA of the a) V-B loop and the b) S_1' Specificity loop in the MD of MMP-1 Co_1•no THP (magneta) and MMP-1 Co_1•no Zn_2 no THP (yellow).

Table S12. Hydrogen bonding interactions observed in the catalytic and structural site of QM/MM optimized structure in MMP-1 Co_1•no THP and MMP-1 Co_1•no Zn_2 no THP.

Atoms			Bond length (Å)	
Donor	DonorH	Acceptor	MMP1-Co_1•no THP	MMP1-Co_1•no Zn_2 no THP
CATALYTIC SITE				
His199-ND1	His199-HD1	Leu216-O	2.78	2.88
His203-N	His203-H	Glu200-O	2.73	2.78
STRUCTURAL SITE				
His177-N	His177-H	His164-O	2.84	2.81
His164-N	His164-H	His177-O	3.00	2.93
His149-ND1	His149-HD1	Asp151-O	Not Present	2.85
Ser153-N	Ser153-H	Asp151-OD1	2.97	3.13

REFERENCES

[1] A. Varghese, S. S. Chaturvedi, G. B. Fields, T. G. Karabencheva-Christova, *J. Biol. Inorg Chem.* **2021**, *26*, 583–597.